33RD CONGRESS
OF THE INTERNATIONAL COUNCIL
OF THE AERONAUTICAL SCIENCES
STOCKHOLM, SWEDEN, 4-9 SEPTEMBER, 2022

ICAS 2022 SWEDEN

EFFICIENT MID-FIDELITY AERODYNAMIC MODELING OF A TILT-WING EVTOL FOR CONTROL APPLICATIONS

Daniel Perdolt[1,2], Daniel Milz[1], Marc May[1] & Moritz Thiele[2]

[1]German Aerospace Center, Institute of System Dynamics and Control, Münchener Straße 20, 82234 Weßling, Germany
[2]Technical University of Munich, Institute of Aircraft Design, Boltzmannstr. 15, 85748 Garching, Germany

Abstract

Urban and regional air mobility have the potential to become important modes of transportation in the future and thus currently attract a lot of attention. Tilt-wing electric vertical takeoff and landing vehicles (eVTOLs) appear to be especially suited in this context as they combine hover capability with efficient cruise flight. However, the development and validation of control concepts require a reasonably accurate yet performant aerodynamic model of the aircraft. In order to obtain representative aerodynamic models of eVTOL aircraft at comparatively low efforts and equipment demands, this work adapts the sequential rapid aero modeling (RAM) process using a mid-fidelity numerical tool *DUST*. Design of experiment and mid-fidelity numerical simulation reduce the computational cost of aerodynamic data generation. Stepwise regression is used to fit the data into a coefficient model. In addition to the total aero-propulsive model, an aerodynamic model decoupled from propulsion forces and moments is identified. The latter is simplified by assuming that the influence of the rotors on the aerodynamic forces and moments depends solely on the thrust. The process is demonstrated on a tandem tilt-wing configuration similar to the Airbus A^3 Vahana, where an aero-propulsive model is efficiently identified. Moreover, a model decoupled from the propulsion forces and moments is obtained. For evaluation, an analysis of aero-propulsive coefficients and a trim study are performed. Two ways to achieve a steady-state transition trajectory are proposed, each using a combination of differential thrust and differential tilt.

Keywords: eVTOL, tilt-wing, aerodynamics, aerodynamic simulation

1 Introduction

Advanced battery and electric propulsion technologies are key developments for urban air mobility and regional air mobility, which are expected to become important modes of transportation in the future [1, 2, 3]. These concepts have the potential to improve travel patterns and thereby significantly shorten travel times [1, 2, 3]. For the intended operations, electric vertical takeoff and landing vehicles (eVTOLs) appear to be particularly advantageous. They allow to reduce the dependence on infrastructures such as runways, providing flexibility for take-off and landing [4, 5]. Tilt-wing and tilt-rotors are subcategories of eVTOLs especially suited for larger flight ranges. Winged flight combined with tilting of the propulsion system promises a compromise with respect to efficiency for both hover and cruise [5].

Despite numerous research efforts, these concepts are not well understood and remain to be analyzed [1]. Their complexity arises from the large design space, the limited availability of empirical data, and the complex aerodynamics [6, 7, 8]. Interactional effects between rotor-rotor, rotor-wing, and wing-rotor impact the aerodynamic performance and behavior. Due to the different flight phases, i.e. hover, transition, and cruise, various aerodynamic effects occur. During transition maneuvers, i.e., from hover to cruise and vice versa, these aerodynamic effects change continuously. In addition, high incidence angles for the rotors and the wings can occur due to wing tilting. Furthermore, it lacks advantageous approaches to perform the transition maneuver between hover and horizontal cruise [9].

However, for the market entry of these eVTOL configurations, it is crucial to maintain safe flight even under non-nominal conditions [10, 11]. That requires fault-tolerant control design, encompassing reliable fault detection, identification, and recovery (FDIR) concepts [10]. Their development and validation demand a reasonably accurate yet capable aerodynamic model of the aircraft [10, 12, 13].

Tilt-wing VTOLs have been part of research for decades. There is research for single wing-rotor combinations [14, 15], single tilt-wing configurations [16, 17], and also on tandem tilt-wing configurations [18, 19, 9, 10]. However, semi-empirical or analytical models have been used primarily for the investigation [13]. The modeling of these systems is mainly performed in the low-fidelity domain, for instance with the aerodynamic tool *VSPAero* [20] based on the vortex lattice method. At the same time, efforts are being made to increase fidelity and efficiency. This includes wind tunnel, flight, and computational testing [21, 22, 23]. CFD simulations are computationally expensive and time-consuming, whereas for flight and wind tunnel tests a functional prototype has to be available, usually associated with high resource requirements.
Nevertheless, these high-fidelity analyses indicate that tilt-wing systems require methods capable of modeling the significant interactions that occur during the transition. A method suitable for efficient analysis and model identification of tilt-wing configurations is presented in [19]. There, momentum theory combined with strip theory is used to capture the effect of propeller-induced slipstream on the wing. However, this yields low complexity of the underlying model and it does not account for rotor-rotor interactions. [19]
A model identification approach using a sequential process to efficiently identify an aerodynamic model has been developed in [24, 25, 12, 13]. However, wind tunnel testing and CFD simulations are used to gather data for the model identification, which poses a resource-intensive step. Still, the process itself is well suited for tilt-wing eVTOL model identification and is thus used in this work.
The tilt-wing configuration of the Airbus A^3 Vahana has already been analyzed using the mid-fidelity aerodynamic tool *DUST*, but no detailed numerical results are provided. Nevertheless, it was demonstrated that the tilt-wing configuration can be adequately analyzed using *DUST*. Besides *DUST*, the *FLOW Lab* "FLOW Unsteady Aerodynamics Suite" is a promising alternative [26]. Like *DUST*, it is based on Vortex Particle Method VPM to model the wake. This is intended to capture fully resolved rotor-rotor, rotor-wing, wing-rotor, and wing-wing interactions [26]. The implemented solver, however, is not yet publicly available.

In this work, the sequential rapid aerodynamic modeling process "RAM" from [25] is adapted for the utilization of a mid-fidelity simulation. The process is intended to efficiently identify aerodynamic models of tilt-wing eVTOL configurations in a fast but still representative manner. Design of Experiment (DoE) significantly reduces the number of simulation points required to cover the aerodynamic envelope space. These points are then simulated with a mid-fidelity numerical tool. The choice of the simulation tool is based on a comparative study of eVTOL rotor analysis tools in [27]. Due to the fidelity requirements, the expected computational cost, and the automation capabilities, the aerodynamic tool *DUST* [28] is chosen, which is publicly available [29]. The particle-based approach promises to capture relevant effects, such as rotor-wing and rotor-rotor interactions. Stepwise regression is performed to efficiently identify a model from the generated data with a polynomial representation. In addition to the aero-propulsive model, a model decoupled from the propulsion system is identified, the aerodynamic model. Propulsion models of any complexity can then be added to this model. Considering most of the explanatory variables for propulsion in the propulsion model rather than in the overall model greatly simplifies the identification process. Complexity is thereby transferred to a propulsion model. The process is demonstrated on a simplified tandem tilt-wing configuration similar to the Airbus A^3 Vahana.

This work is structured as follows: In section 2, the tandem tilt-wing application is performed. Thereby, all steps of the model identification process are explained. The identified aero-propulsive model is analyzed in section 3. In section 4 the results are summarized, and a conclusion is drawn.

2 Tilt-Wing Model Identification

In this section the process shown in fig. 1 is applied to a tilt-wing eVTOL configuration. The individual steps are explained in more detail by applying them to the tilt-wing eVTOL application.

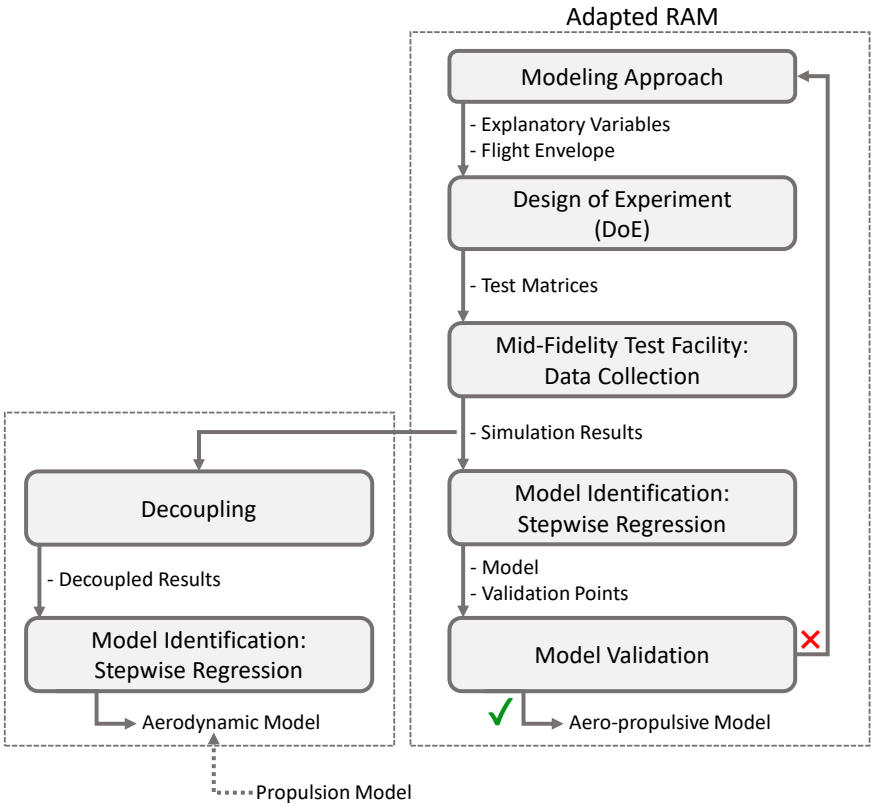

Figure 1 – Overview of the model identification process that integrates mid-fidelity numerical simulations.

2.1 Configuration Description

The investigated tilt-wing configuration is inspired by the Airbus A^3 Vahana but simplified by only considering the wings and rotors. The main wing has a span of $b_m = 6.25$ m and a chord length of $c_m = 0.9$ m. For the canard wing it yields $b_c = 6$ m and $c_c = 0.67$ m. The 25 %-lines of the two wings have a horizontal distance of 4.4 m and a vertical distance of 1.11 m. All dimensions can be found in [30]. The fuselage is neglected since it causes solver problems in *DUST*. Here, it is assumed that aerodynamic characteristics are mainly determined by wings and rotors. Therefore, it is acceptable to neglect the fuselage. The resulting eVTOL tilt-wing configuration is a tandem tilt-wing and shown in fig. 2. The main wing is equipped with two winglets for lateral stabilization. Eight rotors, $n = 8$, are distributed equally on canard and main wing and remain aligned with them during tilt actuation. The sense of rotation of individual rotors can be seen in fig. 2 and is taken from the patent [31].

In a first approach, a *NACA0012* airfoil is assumed for all lifting surfaces. The collective rotor pitch $\theta = 10°$ is kept constant throughout the transition maneuver. The resulting total forces and moments are expressed with respect to the center of gravity. In a first step, this is set in the XZ plane at the center point between the 25 % chord lines of canard and main wing.

2.2 Modeling Approach

For the present application, the explanatory variables are composed of variables that account for the inflow conditions and variables that represent the aircraft actuation systems. For the explanatory variables of the inflow, the fixed-wing convention is applied, using the freestream velocity V_∞, the angle of attack α, and the sideslip angle β. However, the aerodynamic angles become undefined when the

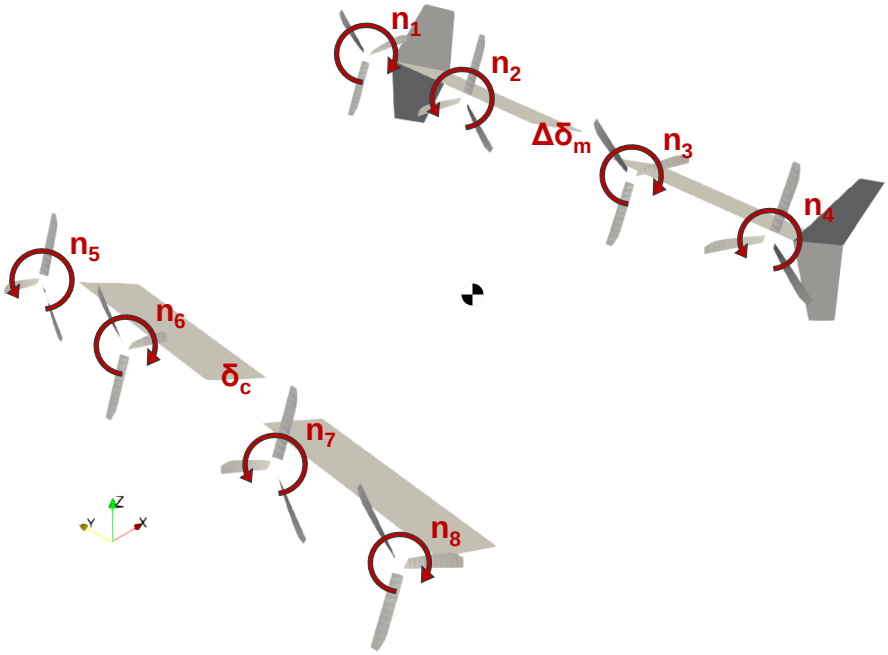

Figure 2 – eVTOL tandem tilt-wing configuration used for the main application.

longitudinal airspeed component approaches zero. Since the focus here is on the transition trajectory, low-speed conditions are disregarded and the fixed-wing convention is applicable. A separate model for the low-speed regime including pure vertical flight is intended. In former applications of the RAM process, rotational rates p,q,r were not considered due to the difficult realization in the wind tunnel [12]. In this work, they are disregarded in order to reduce the design space. The assumption is made that they do not significantly affect the overall aerodynamics for this application. Nevertheless, inflow due to angular rates influences the rotor aerodynamics. Due to the decoupling of the propulsion forces and moments from the model, it is reasonable to neglect the angular rates for aerodynamic considerations while maintaining their influence on the rotors in a separate propulsion model. The remaining explanatory variables describe the vehicle actuators and encompass the tilt angle of the canard wing δ_c, the tilt angle of the main wing with respect to the canard wing $\Delta\delta_\mathrm{m}$, and the rotational velocities of the eight rotors $n_1 \dots n_8$. Here, $\Delta\delta_\mathrm{m}$ prevents unrealistic scenarios with large differences in tilt angles that may occur due to DoE. In contrast, the assignments of rotor speeds $n_1 \dots n_8$ are independent of each other. Modeling of flaps and control surfaces was only recently introduced to *DUST* and is therefore not covered in this work [32]. The resulting actuation-related explanatory variables are shown in fig. 2.

The convention for fixed-wing aircraft, assuming non-dimensional coefficients inversely proportional to the freestream dynamic pressure, is not applied for the response variables because it is invalid for propulsion-dominated vehicles [14, 12]. It is also not applicable if significant interactions between the airframe and propulsion occur [12]. Instead, the dimensional forces $F_\mathrm{x}, F_\mathrm{y}, F_\mathrm{z}$ and moments $M_\mathrm{x}, M_\mathrm{y}, M_\mathrm{z}$ are considered to describe the response variables. The explanatory variables and the response variables comprise a mixed approach for system identification, which is summarized in table 1.

Table 1 – System identification approach for the tandem tilt-wing configuration

Approach	Mixed
Explanatory variables	V_∞, α, β, δ_c, $\Delta\delta_\mathrm{m}$, n_1, n_2, n_3, n_4, n_5, n_6, n_7, n_8
Response variables	F_x, F_y, F_z, M_x, M_y, M_z

The input space is defined as a compromise between the goal to cover a large part of the flight envelope and limitations of the simulation tool in combination with DoE. For the eVTOL tilt-wing

configuration, the flight envelope from early transition flight to cruise flight shall be covered by the model. In order to avoid inconsistent simulation setups provided by DoE, the parameter ranges need to be limited compared to the ranges expected at these flight states. Here, a reliable model at the cost of decreased flight envelope coverage is preferred. As an alternative, either multiple linear design spaces or a nonlinear transformation of a linear space could be used. The respective parameter limits for the selected region of the flight envelope are shown in table 2.

Table 2 – Flight envelope intended to cover early transition to cruise flight: feasible parameter range

Expl. variables	**Minimum**	**Maximum**
$\boldsymbol{V_\infty}$	$10\ \mathrm{m\,s^{-1}}$	$60\ \mathrm{m\,s^{-1}}$
$\boldsymbol{\alpha}$	-5°	10°
$\boldsymbol{\beta}$	-3°	3°
$\boldsymbol{\delta_\mathrm{c}}$	0°	30°
$\boldsymbol{\Delta\delta_\mathrm{m}}$	-10°	10°
$\mathbf{n_1}$ - $\mathbf{n_8}$	$600\ \mathrm{min^{-1}}$	$5000\ \mathrm{min^{-1}}$

The minimum of V_∞ is chosen to be reasonable for a flight state in early transition. The maximum V_∞ is chosen to be slightly higher than the expected cruise speed of the Vahana. Compared to conventional aircraft, the ranges of α and β are chosen to be relatively large. For vehicles with VTOL capabilities, larger sideslip angles can occur at low flight speeds and strong winds. But again, conservative limits are preferred. By definition, the wings are oriented horizontally for $\delta_\mathrm{c} = \delta_\mathrm{m} = 0^\circ$. A differential tilt angle of $\Delta\delta_\mathrm{m} = 0^\circ$ corresponds to an identical wing tilt of canard and main wing. The ranges of δ_c and $\Delta\delta_\mathrm{m}$ are based on investigations in [30]. The aerodynamic solution in *DUST* diverges at post-stall conditions ($\alpha + \delta$ above 50°). The choice of the minimum and maximum n is likewise based on the insights from [30].

2.3 Data Generation

Based on the explanatory variables (table 1) and the corresponding ranges (table 2), DoE provides a test plan for the efficient exploration of the spanned 13-dimensional design space. The deployed methods in the course of DoE application reflect the intended order of the resulting model. Fractional factorial design (FFD) [33] covers linear relationships between all parameters. That is extended to second-order modeling using additional center points provided by central composite design (CCD) [33]. To explore the inner design space, nearly orthogonal latin hypercubes (NOLH) [33, 34, 35] are deployed. A sufficiently high number of NOLH points avoids an underdetermined system of equations for third-order polynomial approximation. Additional NOLH points are exclusively generated for validation.

The mid-fidelity numerical tool *DUST* is employed to simulate the test and validation points specified by DoE in order to generate the data for the subsequent system identification process.

Comprehensive preliminary tests are described in [30]. The configuration shown in fig. 2 is configured in *DUST*, whereas the choice of component modeling is again described in [30]. The eight rotors are modeled using a lifting line method (LL). All remaining lifting surfaces, i.e. all wings and winglets, are also modeled with LL. The wake is modeled by vortex particles. This selection process is an iterative process and studies are carried out for key parameters. These studies and all resulting simulation parameters are described in [30]. After configuration creation and simulation setup, all flight conditions provided by the DoE are simulated. Fig. 3 shows three simulation points representing different phases of the transition flight.

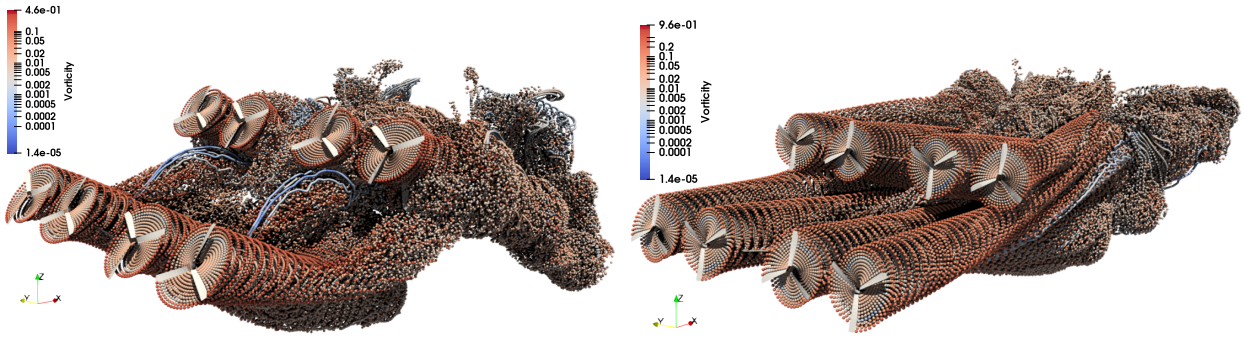

(a) Early transition at $\delta_c = \delta_m = 45°$ and $V_\infty = 10\,\mathrm{m\,s^{-1}}$ (b) Mid transition at $\delta_c = \delta_m = 20°$ and $V_\infty = 20\,\mathrm{m\,s^{-1}}$

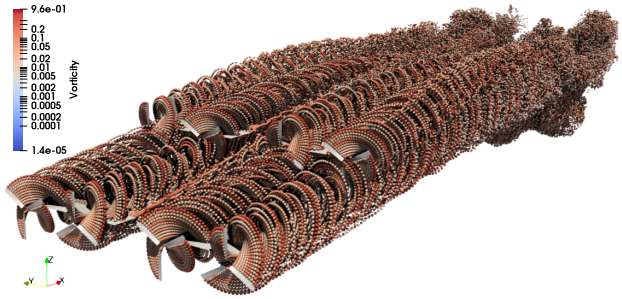

(c) Cruise flight at $\delta_c = \delta_m = 4°$ and $V_\infty = 55\,\mathrm{m\,s^{-1}}$

Figure 3 – Visualization of numerical simulations of different tilt-wing configuration flight states performed with *DUST*.

The representation of the wake with vortex particles indicates the various interactions that occur. In early transition (fig. 3a), there is interference between the canard wake and the main wake despite high tilt angles. The slipstream of the canard is deflected by interaction with the freestream and causes an upwash and high angles of attack at the main wing. The inflow of rotors at the main wing, in contrast, is not directly affected. The opposed rotation of rotors in combination with high incidence angles appears to result in a coupled vortex shedding from the canard wake, as indicated here by two blue arcs of particles. This behavior is not seen for moderate tilt angles in neither fig. 3b nor fig. 3c. For the mid-transition case, interaction between main and canard wing-rotor components shows to be reduced by the vertical geometrical offset. As can be seen, the interaction of slipstream with the tip vortex is included in the simulation, causing the wake of outer rotors to rotate inwards. Strong turbulence is present after the mixing of canard and main wing wakes. In cruise flight, the high-speed wake of the canard wing and respective rotors acts almost frontally on the main wing rotors and the main wing itself. As both slipstream and the freestream are aligned, no strong lateral or vertical turbulences can be observed. In contrast to fig. 3b, slipstream contraction is less prominent in cruise, because the effect of flow acceleration is small compared to the high total velocity. However, diffusion between the slipstream tube and the surrounding air is visible in the transition from near- to far-wake.

2.4 Model Identification: Stepwise Regression

The data obtained for the DoE points is used to identify an aero-propulsive model. Stepwise regression [36] is performed with an entry criterion $P_{\text{in}} = 0.95$ and an exit criterion $P_{\text{out}} = 0.95$ for the partial F-test. Terms up to the 3$^{\text{rd}}$ order are considered. These settings have been examined in [30]. An aero-propulsive model in polynomial representation is generated. The forces and moments are obtained as a function of the vehicle state and control variables.

Table 3 provides a summary of the resulting modeling metrics. Here, p represents the number of regressors and DoF the degrees of freedom. ${R^2}_m$ denotes the modeling coefficient of determination and ${R^2}_{adj,m}$ is the adjusted modeling coefficient of determination. $NRMSE_m$ denotes the modeling

Table 3 – Modeling metrics for 3rd order stepwise regression to identify the aero-propulsive model

	$\mathbf{F_x}$	$\mathbf{F_y}$	$\mathbf{F_z}$	$\mathbf{M_x}$	$\mathbf{M_y}$	$\mathbf{M_z}$
p	102	41	40	61	42	86
DoF	498	559	560	539	558	514
$\mathbf{R^2_m}$	0.999	0.902	0.987	0.923	0.970	0.990
$\mathbf{R^2_{adj,m}}$	0.999	0.895	0.986	0.915	0.968	0.988
$\mathbf{NRMSE_m}$ $(\%)$	0.594	5.003	2.021	2.993	3.073	1.115

normalized root mean squared error, whereas the normalization is performed by the range of the respective response variable. The modeling metrics are adequate for the identification of the aero-propulsive model. However, these metrics provide limited information about the predictive capabilities of the identified model.

The identified model is therefore tested by means of a prediction error test using validation points. For this purpose, an error threshold is defined. Former applications of the RAM process use a prediction error threshold of $\varepsilon_{th} = 5\ \%$ [12] when comparing validation data to model prediction. The prediction error ε is normalized over the range of simulation results for each output variable. In table 4, the mean and standard deviation for the normalized prediction errors ε^* are given for all response variables.

Table 4 – Normalized prediction error: Mean value and standard deviation for the validation points

	$\mathbf{F_x}$	$\mathbf{F_y}$	$\mathbf{F_z}$	$\mathbf{M_x}$	$\mathbf{M_y}$	$\mathbf{M_z}$
ε^* $(\%)$	0.777 $\pm$ 0.611	0.294 $\pm$ 0.298	2.026 $\pm$ 1.823	1.822 $\pm$ 1.159	4.467 $\pm$ 4.432	1.169 $\pm$ 1.026

The mean of ε^* is lower than the defined threshold of $\varepsilon_{th} = 5\ \%$ for all response variables. However, F_z and M_y show a relatively high standard deviation for ε^*. This is due to higher-order nonlinear effects resulting from stall. These cannot be captured by the 3rd order stepwise regression.

The prediction error test demonstrates the ability of the model to predict the data provided by *DUST*. The capability of the model to represent realistic data remains to be evaluated in section 3 with the analysis of the aero-propulsive model.

2.5 Decoupling of Propulsion Forces and Moments

Next to the aero-propulsive model, a decoupled aerodynamic model is identified. That allows to shift modeling complexity of propulsive dependencies from the total model to isolated rotor models, thereby reducing the dimensionality of the input space. Explanatory variables that can be shifted are the body rotational rates p, q, r, the variable blade pitch, and the rotational speed n_i of each rotor.
To obtain a non-propulsive representation of the aircraft, propulsion forces and moments are subtracted from the aero-propulsive response obtained in *DUST*:

$$T_{\text{i}} = F_{\text{x,rotor i,hub i}} \tag{1a}$$

$$\hat{F} = F - \sum_{i=1}^{n} F_{\text{rotor i,body}} \tag{1b}$$

$$\hat{M} = M - \sum_{i=1}^{n} M_{\text{rotor i,body}} \tag{1c}$$

Here, $\hat{F}$ and $\hat{M}$ are the decoupled force and moment, respectively. The relevant propulsion data, $F_{\text{x,rotor i,hub i}}$, $F_{\text{x,rotor i,body i}}$, and $\text{M}_{\text{rotor,i,body}}$, is directly provided by *DUST* in both the body and hub

frame for each rotor with index i. That means that no additional data acquisition is necessary, making the decoupling a pure post-processing step with low effort. Although the ambition is to exclude the propulsion response from the system, the impact of rotor slipstream on the flow field is still present in the aerodynamic behavior and must be considered [12]. Assuming that the wake of the rotors can solely be characterized by thrust T according to momentum theory [15], the respective thrusts $T_1 - T_n$ enter the model identification as new explanatory variables to describe the propulsion-dominated flow field.

After the decoupling is applied to the complete data set, the aerodynamic model can be identified analogously to the aero-propulsive model. The respective system identification approach is summarized in table 5. Adequate modeling metrics are obtained, as can be seen in table 6. For $\hat{M}_x$, $R^2_{adj,m}$ is considerably lower in comparison to all other response variables. This can result from the lack of propulsion-generated moment around x after decoupling, which makes the identification of this variable problematic. For $\hat{M}_z$ this behavior is less apparent.

Table 5 – System identification approach after decoupling

Approach	(Decoupled) aerodynamic model
Explanatory variables	V_∞, α, β, δ_c, $\Delta\delta_m$, T_1, T_2, T_3, T_4, T_5, T_6, T_7, T_8
Response variables	$\hat{F}_x$, $\hat{F}_y$, $\hat{F}_z$, $\hat{M}_x$, $\hat{M}_y$, $\hat{M}_z$

Table 6 – Modeling metrics for 3rd order stepwise regression to identify the aerodynamic model.

	$\hat{\mathbf{F}}_x$	$\hat{\mathbf{F}}_y$	$\hat{\mathbf{F}}_z$	$\hat{\mathbf{M}}_x$	$\hat{\mathbf{M}}_y$	$\hat{\mathbf{M}}_z$
p	50	49	43	46	46	56
DoF	550	551	557	554	554	544
$\mathbf{R^2_m}$	0.998	0.929	0.992	0.766	0.980	0.914
$\mathbf{R^2_{adj,m}}$	0.998	0.923	0.991	0.747	0.978	0.905
$\mathbf{NRMSE_m}$ (%)	1.006	4.633	1.851	4.893	2.498	5.111

A limitation to note is that while the rotor thrusts are included in the data model, the superimposed flow is not quantifiable. If a separate propulsion model would be added, however, the inflow would be required to be considered as input among other parameters. The superposition of free and propeller-induced flow is intrinsically included in the (decoupled) aerodynamic model.

3 Tilt-Wing Model Analysis

Since no validation data is publicly available for this tandem tilt-wing configuration, the identified model is tested by various other means. First, the aero-propulsive coefficients are compared to available coefficients of a single wing-rotor combination. Then, a trim study is performed and qualitatively compared with trim trajectories from other studies. Thereby, different trim approaches are analyzed and it is investigated which approaches can be realized with the identified model.

3.1 Aero-propulsive Coefficients Analysis

For wings that are largely immersed in the slipstream of a rotor, the forces and moments on the wing are influenced by the dynamic pressure in the slipstream $\bar{q}_s$ [15]. Therefore, it is not valid for propulsion-dominated configurations to determine the dimensionless coefficients via the dynamic pressure of the inflow. According to Kuhn and Draper [15], it is reasonable to consider $\bar{q}_s$ for the coefficients. It is assumed that the $\bar{q}_s$ is related to the thrust via the momentum theory [15] as

$$\bar{q}_s = \frac{1}{2}\,\rho {V_\infty}^2 + \frac{T}{S_d} \tag{2}$$

where S_d denotes the rotor disk area and ρ the local air density. Using $\overline{q}_\mathrm{s}$, the slipstream lift coefficient $C_{\mathrm{L_s}}$, the slipstream coefficient to describe the forces in x-direction $C_{\mathrm{X_s}}$, and the slipstream thrust coefficient $C_{\mathrm{T_s}}$ can be derived according to [15] as

$$C_{\mathrm{L_s}} = \frac{L}{\overline{q}_\mathrm{s} S} \tag{3a}$$

$$C_{\mathrm{X_s}} = \frac{D - T_\mathrm{x}}{\overline{q}_\mathrm{s} S} \tag{3b}$$

$$C_{\mathrm{T_s}} = \frac{T}{\overline{q}_\mathrm{s} S_\mathrm{d}} = \frac{T/S_\mathrm{d}}{T/S_\mathrm{d} + \overline{q}} \tag{3c}$$

with the inflow dynamic pressure $\overline{q} = \frac{1}{2}\,\rho {V_\infty}^2$.

Fig. 4a shows the $C_{\mathrm{L_s}}$ curve for different $C_{\mathrm{T_s}}$. Increasing $C_{\mathrm{T_s}}$ implies increasing contribution of the thrusts $T_{1\text{-}8}$ to $\overline{q}_\mathrm{s}$. It can be observed that with higher $C_{\mathrm{T_s}}$ the onset of stall, recognizable by the drop in $C_{\mathrm{L_s}}$, is delayed. This behavior can be observed in fig. 4a. It can also be observed that, despite the symmetrical profiles employed, $C_{\mathrm{L_s}}\big|_{\delta=0} \neq 0$ is present in some cases. This is considered to be caused by the influence of the canard wing and rotor wake on the main wing.

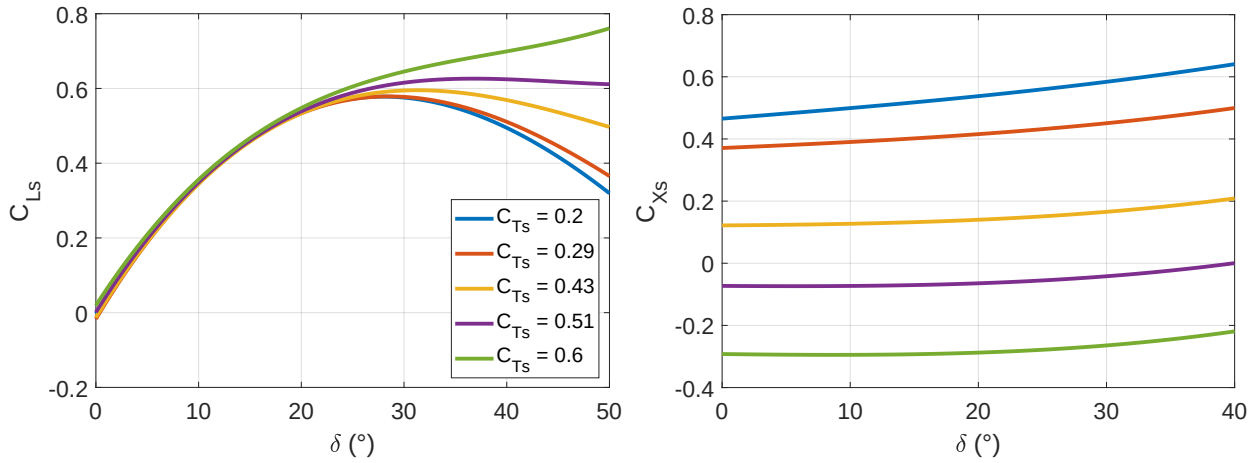

(a) $C_{\mathrm{L_s}}$ vs. δ

(b) $C_{\mathrm{X_s}}$ vs. δ

Figure 4 – Aero-propulsive coefficients for different $C_{\mathrm{T_s}}$ for $\alpha = 0°$.

In fig. 4b, $C_{\mathrm{X_s}}$ is plotted for different thrust settings defined by $C_{\mathrm{T_s}}$. The $C_{\mathrm{X_s}}$ curve is shifted downwards with increasing $C_{\mathrm{T_s}}$, which shows that the thrust increasingly exceeds the drag. The increasing behavior of $C_{\mathrm{X_s}}$ with increasing δ is present. However, this is not reflected adequately in this representation. This is only due to the representation of several curves, which are shifted differently along the y-axis depending on the $C_{\mathrm{T_s}}$.

Similar characteristics could be observed in wind tunnel tests and in analytical calculations for a single rotor-wing combination, described in [15] and [14]. Therefore, the results indicate that the described characteristics can be transferred from a single rotor-wing combination to a tandem tilt-wing configuration. However, an influence of the canard wing on the main wing is present.

3.2 Trim Study: Theoretical Analysis

There is currently a lack of understanding on how to accomplish the transition maneuver between hover and horizontal flight efficiently [9]. This section investigates the transition maneuver along a steady-state trajectory analytically. This gives basic knowledge of tandem tilt-wing trimming which can subsequently be used as a comparison for the trim study performed with the aero-propulsive model. Depending on the progress in the transition maneuver, the propulsive forces are needed to provide lift and overcome the drag. In a first approach, the trim analysis is limited to longitudinal

motion. Therefore, only the longitudinal forces F_x and F_z and the pitching moment M_y are relevant for this calculation. It is assumed, however, that the equilibria for F_x and F_z are ensured. The pitching moment equilibrium is considered to be the critical factor for the trim of a tilt-wing configuration.

The goal of this study is to find steady-state solutions for given constraints. Thus, operating points for which the pitching moment vanishes (i.e., $M_y = 0$) are sought. There are three approaches to achieve a trimmed trajectory of a tandem tilt-wing. The trimming could be realized exclusively by differential thrust between main and canard wing, controlled by the respective rotor speeds $n_{1\text{-}4}$ and $n_{5\text{-}8}$. Here, the main wing is tilted analogously to the canard wing. In another approach, the trimming is realized via a differential tilt of the canard wing and the main wing, described by $\Delta\delta_m$. In this case, the rotational speeds of the rotors of the canard wing are set equal to those of the main wing. A coupling of the two approaches is also conceivable, although it is more complex with regard to the influencing variables. Which approach is preferable depends on the control strategy and limitations due to design and configuration.

Fig. 5 shows the configuration with all relevant forces, moments and geometrical parameters.

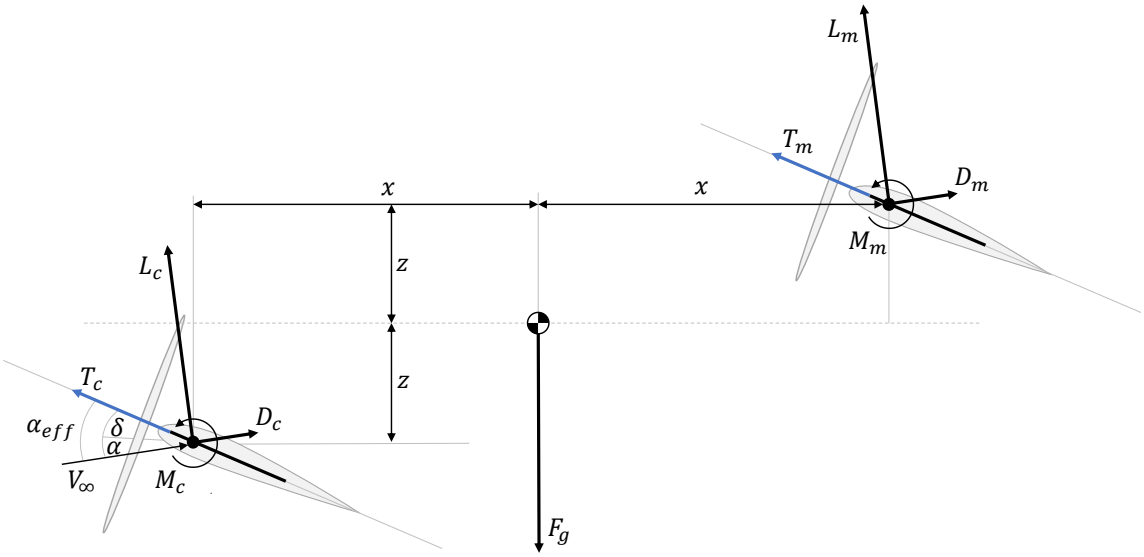

Figure 5 – All considered forces acting on the wings of the tandem tilt-wing configuration.

The pitching moment equilibrium considering geometry constraints is:

$$\begin{aligned}\sum M_y \stackrel{!}{=} 0 =& M_c + M_m + \sin(\alpha)\left[z(L_c - L_m) + x(D_c - D_m)\right] + \cos(\alpha)\left[x(L_c - L_m) - z(D_c - D_m)\right] \\ &+ \cos(\delta_c)\, T_c z - \cos(\delta_m)\, T_m z + \sin(\delta_c)\, T_c x - \sin(\delta_m)\, T_m x \\ =& M_C + M_M + \sin(\alpha)\left[-z\Delta L - x\Delta D\right] + \cos(\alpha)\left[-x\Delta L + z\Delta D\right] \\ &+ \cos(\delta_c)\, T_c z - \cos(\delta_m)\, T_m z + \sin(\delta_c)\, T_c x - \sin(\delta_m)\, T_m x\end{aligned} \tag{4}$$

where $\Delta L = L_m - L_c$ and $\Delta D = D_m - D_c$ are the differences in lift and drag between main and canard wing. It is expected that for a symmetric airfoil, the slipstream-induced lift can be neglected and the slipstream-induced drag is always opposed to the thrust and is orders smaller than the thrust, and thus can be neglected as well. Now assuming that the respective airfoil pitching moments M_c and M_m are small, and using small-angle approximation for α yields:

$$0 = -\Delta L(x + \alpha z) + \Delta D(z - \alpha x) + \cos(\delta_c)\, T_c z - \cos(\delta_m)\, T_m z + \sin(\delta_c)\, T_c x - \sin(\delta_m)\, T_m x \tag{5}$$

Replacing $\delta_c = \delta$, and $\delta_m = \delta + \Delta\delta_m$ while assuming small $\Delta\delta_m$ yields:

$$0 = -\Delta L(x + \alpha z) + \Delta D(z - \alpha x) + \Delta T\left[z\cos(\delta) + x\sin(\delta)\right] - \Delta\delta_m\left[\cos(\delta)\, T_m x + \sin(\delta)\, T_m z\right] \tag{6}$$

$$\Longleftrightarrow \Delta L(x + \alpha z) - \Delta D(z - \alpha x) = \Delta T\left[z\cos(\delta) + x\sin(\delta)\right] - \Delta\delta_m T_m\left[x\cos(\delta) + z\sin(\delta)\right] \tag{7}$$

This represents a simplified formulation but considers both major trim options: differential thrust ΔT and differential tilt $\Delta\delta_m$. Lift and drag terms are functions of $\alpha_{eff} = \delta + \alpha$ and the magnitude of the respective terms depends on the flight phase. It is worth noting that differential tilt affects the aerodynamic terms via the coefficients. For near-cruise conditions, $\Delta L > \Delta D$, a negative contribution of the freestream angle of attack to the pitching moment (positive left side of eq. (7)) can be observed. The moment needs to be canceled by the actuation variables on the right side. This relation is inverted close to hover conditions (for $\delta > 80°$). A positive $\Delta\delta_m$, meaning that $\delta_m > \delta_c$, results in a negative pitching moment. To cancel the negative freestream aerodynamic pitching moment, $\Delta\delta_m$ thus must be negative. The geometry and tilt angle term for ΔT is always positive, wherefore a positive differential thrust can cancel the negative aerodynamic pitching moment. These considerations show that, assuming higher aerodynamic forces on the main wing $\Delta L, \Delta D > 0$, $T_c > T_m$ or $\delta_c > \delta_m$ or a combination of them can be used to balance pitching moment beyond early transition.

To provide more insight into the inversion of aerodynamic pitching moment, the formulation is further simplified by merely considering differential thrust and assuming $\Delta\delta_M = 0$. The aerodynamic forces ΔL and ΔD are replaced with their coefficient definitions:

$$\Delta L = L_m - L_c = \frac{\rho}{2} V_\infty^2 C_L (S_m - S_c) \tag{8}$$

$$\Delta D = D_m - D_c = \frac{\rho}{2} V_\infty^2 C_D (S_m - S_c) \tag{9}$$

The aerodynamic coefficients are a function of the effective angle of attack, which is equal for main and canard without differential tilt angle. Thus $C_{L,M} = C_{L,C} = C_L$ and $C_{D,M} = C_{D,C} = C_D$. This results in:

$$\Delta L (x + \alpha z) - \Delta D (z - \alpha x) = \frac{\rho}{2} V_\infty^2 (S_m - S_c) \underbrace{[C_L (x + \alpha z) - C_D (z - \alpha x)]}_{R} \tag{10}$$

As $S_m > S_c$ due to design, the sign inversion is determined by the term in square brackets, referred to as R. The decisive term R is plotted in fig. 6.

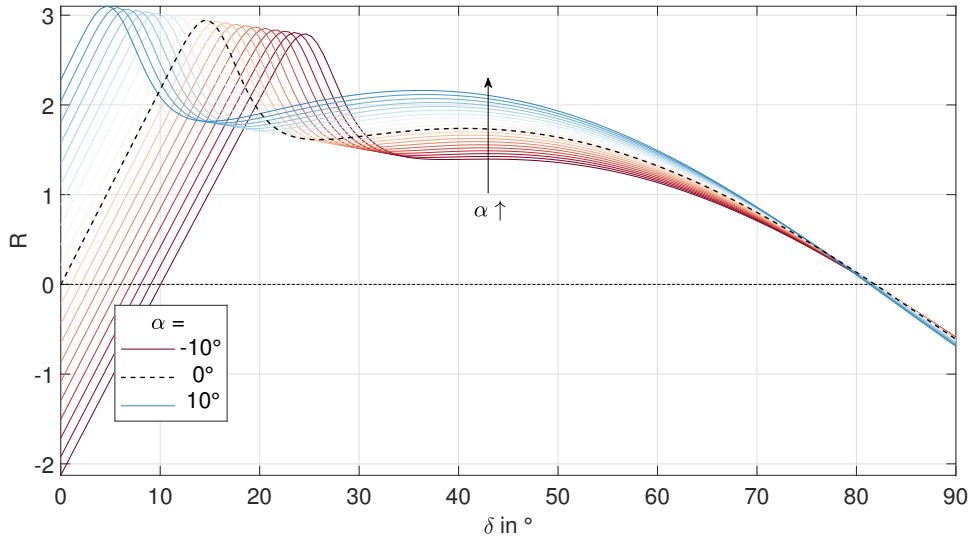

Figure 6 – Investigation of the inversion of the aerodynamic pitching moment.

As can be seen, R is consistently ≥ 0 for the range to be covered by the model when assuming positive angles of attack. This demonstrates the considerations made that $T_c > T_m$ must follow to balance the pitching moment for this configuration. Sign conversion occurs at $\delta > 80°$ in near-hover conditions. The angle of attack does not have a strong influence on the location of this zero crossing. For moderate angles of attack, the term of R diminishes in cruise conditions when δ approaches zero.

3.3 Trim Study: Aero-propulsive Model

Using the previously identified aero-propulsive model, it is investigated which trim approaches can be realized. A nonlinear programming solver to find the minimum of a constrained nonlinear multivariable function is applied.

For a given velocity $V_\infty \in [10\ \mathrm{m\,s^{-1}};\ 60\ \mathrm{m\,s^{-1}}]$, optimal values $x^* = [\alpha^*, \delta^*, n^*]$ are sought.

$$x^* = \arg\min_x \left\| \begin{matrix} F_\mathrm{x}(x,\ldots) \\ F_\mathrm{z}(x,\ldots) - F_\mathrm{g} \\ M_\mathrm{y}(x,\ldots) \end{matrix} \right\|_2 \tag{11}$$

where $F_\mathrm{x}, F_\mathrm{z}, M_\mathrm{y}$ are functions of V_∞, α, β, δ_c, $\Delta\delta_\mathrm{m}$, $n_1 \ldots n_8$ and F_g is the gravitational force to be compensated.

In the tests performed, trimming of the entire intended transition trajectory was not feasible using exclusively one approach. Trimming solely by differential thrust could not be achieved over any range. The nose-down moment present can be equalized, but beyond that, no sufficient thrust can be ensured throughout the flight envelope. Trimming by differential tilt is only suitable for mid and late transition up to cruise flight. A smaller tilt angle of the main wing compared to the canard wing ($\delta_m < \delta_c$) is recommended for this specific configuration. However, the combination of differential thrust and differential tilt, on the other hand, allows trimming starting from $V_\infty \approx 36\ \mathrm{m\,s^{-1}}$. No trimming could be realized for lower speeds. This is due to the constraint of the tilt angles from section 2.2. For trimming at low V_∞, relatively high δ_c and δ_m would be required, which did not produce valid simulation results when using *DUST*.

For the combination of differential thrust and differential tilt, two trim trajectories are proposed, shown in fig. 7 and 8. The first proposed trajectory is shown in fig. 7. It is implemented in such a way that, if possible, trimming is realized by differential tilt. In fig. 7b it is evident that trimming solely by differential tilt is only possible starting from $V_\infty \approx 44\ \mathrm{m\,s^{-1}}$. However, a δ_c up to $-10°$ is required, as it can be observed in the fig. 7a. Before $44\ \mathrm{m\,s^{-1}}$ trimming is only achievable when additionally using differential thrust.

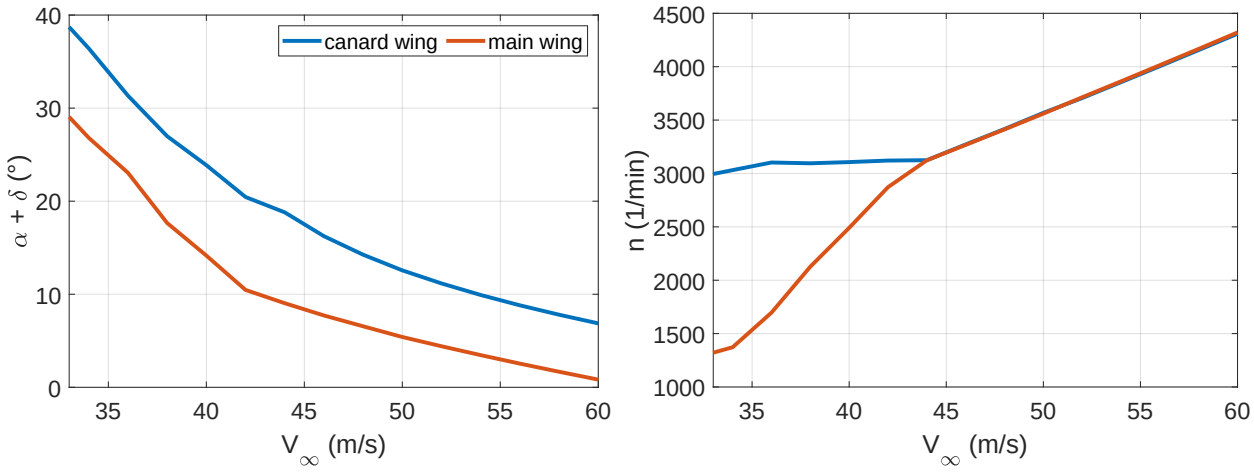

(a) $\alpha + \delta$ vs. V_∞ (b) n vs. V_∞

Figure 7 – Trim study for the aero-propulsive model of the tilt-wing configuration - Proposal 1.

The second proposed trajectory is presented in fig. 8. In this case, the trimming is preferably achieved through the differential thrust and the differential tilt is kept as low as possible. Complete trimming by differential thrust alone is not achievable for any range. Furthermore, a relatively high difference in rotational speed between canard and main wing is required. This difference is apparent in fig. 8b. Nevertheless, fig. 8a indicates that a reduced δ is required compared to fig. 7a.

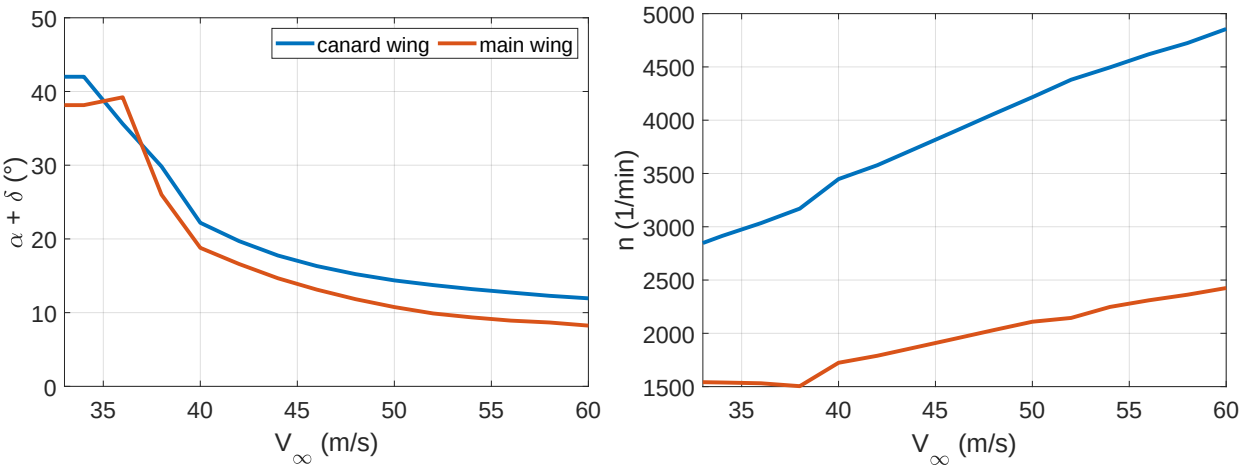

(a) δ vs. V_∞ (b) n vs. V_∞

Figure 8 – Trim study for the aero-propulsive model of the tilt-wing configuration - Proposal 2.

The considerations from section 3.2 that pitching moment trimming is expected via $\Delta L, \Delta D > 0$, $T_c > T_m$ and/or $\delta_c > \delta_m$ can be observed. Furthermore, the qualitative behavior of both proposed trajectories is comparable to trim trajectories in other studies. It is comparable to those of a single wing-rotor combination [14] and to those of a single tilt-wing configuration [16]. It can also be compared to tandem tilt-wing trim trajectories from [9, 37, 10, 18]. It should be mentioned that in [9], however, trimming was only possible via differential thrust. This is in contrast to the results of this work. The main reason for this could be the center of gravity position, which is further aft for the configuration used in [9]. The aft center of gravity position could allow this trimming via differential thrust to be facilitated. A higher positive moment could be generated via the thrust of the canard wing.

4 Conclusion

The presented adapted process enables the identification of aero-propulsive and aerodynamic models with medium fidelity. The mid-fidelity numerical simulations allow for a more efficient and time-saving model identification compared to e.g. CFD, wind tunnel, and flight testing. The process is intended for and was demonstrated using a tandem tilt-wing eVTOL configuration. This configuration represents a simplified version of the Airbus A^3 Vahana. An aero-propulsive model and an aerodynamic model with adequate modeling metrics were identified and serve as a suitable base for control tasks.

The aero-propulsive coefficients of the identified aero-propulsive model are comparable to coefficients of a single wing-rotor combination. In addition, the influence of the wake of the canard wing and its rotors on the main wing can be observed. However, the model cannot represent behavior exceeding 3$^{\text{rd}}$ order interactional terms. This limitation is relevant for the complex post-stall behavior but could be addressed using a regression method that is capable of considering higher-order effects. Applying the model to a trim study demonstrated that trimming of the majority of the intended flight envelope is feasible with a combination of differential tilt and differential thrust. $T_c > T_m$ and $\delta_c > \delta_m$ are suggested, for which two ways are proposed. $T_c > T_m$ and $\delta_c > \delta_m$ is in agreement with a theoretical evaluation. Trimming solely by differential tilt could not be achieved over any range. Trimming by differential thrust could only be realized for mid transition to cruise flight. In general, the identified model is not valid for early transition flight. For small inflow velocities ($V_\infty < 35\ \mathrm{m\,s^{-1}}$), trimming is not feasible. This limitation results from a necessary restriction of the tilt angles, as the used aerodynamic solver cannot realistically represent flight states with very high tilt angles. A valid representation of hover and early transition remains to be established. However, for flight conditions between mid transition and cruise flight, the model indicates reasonable behavior. Nevertheless, in this process, no real data but simulation data is used to identify the models. To make an assessment of the accuracy and physical quality of the models, a comparison with real data is required.

5 Contact Author Email Address

mailto: daniel.perdolt@dlr.de

6 Copyright Statement

References

[1] R. Rothfeld, A. Straubinger, M. Fu, C. Al Haddad, and C. Antoniou. Urban air mobility. In *Demand for Emerging Transportation Systems*, pages 267–284, 2020. doi: 10.1016/B978-0-12-815018-4.00013-9.

[2] S. Roy, A. Maheshwari, W.A. Crossley, and D.A. DeLaurentis. Future regional air mobility analysis using conventional, electric, and autonomous vehicles. *Journal of Air Transportation*, 29(3), 2021. doi: 10.2514/1.D0235.

[3] M. Fu, R. Rothfeld, and C. Antoniou. Exploring preferences for transportation modes in an urban air mobility environment: Munich case study. *Transportation Research Record: Journal of the Transportation Research Board*, 2673(10):427–442, 2019. doi: 10.1177/0361198119843858.

[4] M. Daskilewicz, B. German, M. Warren, L.A. Garrow, S. Boddupalli, and T.H. Douthat. Progress in vertiport placement and estimating aircraft range requirements for evtol daily commuting. In *2018 Aviation Technology, Integration, and Operations Conference*, 2018. doi: 10.2514/6.2018-2884.

[5] S. Chauhan and J. Martins. Tilt-wing evtol takeoff trajectory optimization. *Journal of Aircraft*, 57(1):93–112, 2020. doi: 10.2514/1.C035476.

[6] A. Bacchini. *Electric VTOL preliminary design and wind tunnel tests*. PhD thesis, Politecnico di Torino, 2020.

[7] T. Stokkermans, D. Usai, T. Sinnige, and L. Veldhuis. Aerodynamic interaction effects between propellers in typical evtol vehicle configurations. *Journal of Aircraft*, 58(4), 2021. doi: 10.2514/1.C035814.

[8] D. Shukla and N. Komerath. Multirotor drone aerodynamic interaction investigation. *Drones*, 2(4):43, 2018. doi: 10.3390/drones2040043.

[9] R.C. Busan, P.C. Murphy, D.B. Hatke, and B.M. Simmons. Wind tunnel testing techniques for a tandem tilt-wing, distributed electric propulsion vtol aircraft. In *AIAA Scitech 2021 Forum*, 2021. ISBN 978-1-62410-609-5. doi: 10.2514/6.2021-1189.

[10] M. May, D. Milz, and G. Looye. Dynamic modeling and analysis of tilt-wing electric vertical take-off and landing vehicles. In *AIAA SCITECH 2022 Forum*, 2022. ISBN 978-1-62410-631-6. doi: 10.2514/6.2022-0263.

[11] D. Milz and G. Looye. Tilt-wing control design for a unified control concept. In *AIAA SCITECH 2022 Forum*, 2022. doi: 10.2514/6.2022-1084.

[12] B.M. Simmons and P.C. Murphy. Wind tunnel-based aerodynamic model identification for a tilt-wing, distributed electric propulsion aircraft. In *AIAA Scitech 2021 Forum*, 2021. doi: 10.2514/6.2021-1298.

[13] B. M. Simmons, P.G. Buning, and P.C. Murphy. Full-envelope aero-propulsive model identification for lift+cruise aircraft using computational experiments. In *AIAA AVIATION 2021 FORUM*, 2021. doi: 10.2514/6.2021-3170.

[14] J. Cook and J. Hauser. Transition to hover for a flying wing with electric propulsion. In *2018 Annual American Control Conference (ACC)*, 2018.

[15] R.E. Kuhn and J.W. Draper. Investigation of the aerodynamic characteristics of a model wing-propeller combination and of the wing and propeller separately at angles of attack up to 90 degrees. 1956.

[16] J. Holsten, T. Ostermann, and D. Moormann. Design and wind tunnel tests of a tiltwing uav. *CEAS Aeronautical Journal*, 2(1-4):69–79, 2011. doi: 10.1007/s13272-011-0026-4.

[17] J. Jeong, S. Yoon, S.K. Kim, and J. Suk. Dynamic modeling and analysis of a single tilt-wing unmanned aerial vehicle. In *AIAA Modeling and Simulation Technologies Conference*, 2015. doi: 10.2514/6.2015-1804.

[18] E. Cetinsoy, C. Hancer, K.T. Oner, E. Sirimoglu, and M. Unel. Aerodynamic design and characterization of a quad tilt-wing uav via wind tunnel tests. *Journal of Aerospace Engineering*, 25(4):574–587, 2012. doi: 10.1061/(ASCE)AS.1943-5525.0000161.

[19] J. Cook. A strip theory approach to dynamic modeling of evtol aircraft. In *AIAA Scitech 2021 Forum*, 2021. ISBN 978-1-62410-609-5. doi: 10.2514/6.2021-1720.

[20] VSPAero. vspaerotutorial [openvsp], 31.03.2022. http://openvsp.org/wiki/doku.php?id=vspaerotutorial.

[21] A.S. Saeed, A. Younes, C. Cai, and G. Cai. A survey of hybrid unmanned aerial vehicles. *Progress in Aerospace Sciences*, 98:91–105, 2018. doi: 10.1016/j.paerosci.2018.03.007.

[22] R. DeLoach. Applications of modern experiment design to wind tunnel testing at nasa langley research center. In *36th AIAA Aerospace Sciences Meeting and Exhibit*, 1998. doi: 10.2514/6.1998-713.

[23] J.R. Simpson and J.W. Wisnowski. Streamlining flight test with the design and analysis of experiments. *Journal of Aircraft*, 38(6), 2001. doi: 10.2514/2.2879.

[24] P.C. Murphy, D. Hatke, V.V. Aubuchon, R. Weinstein, and R.C. Busan. Preliminary steps in developing rapid aero modeling technology. In *AIAA Scitech 2020 Forum*, 2020. doi: 10.2514/6.2020-0764.

[25] B.M. Simmons. System identification for propellers at high incidence angles. In *AIAA Scitech 2021 Forum*, 2021. doi: 10.2514/6.2021-1190.

[26] Alvarez E.J. and Ning A. Modeling multirotor aerodynamic interactions through the vortex particle method. In *AIAA Aviation 2019 Forum*, 2019. doi: 10.2514/6.2019-2827.

[27] D. Perdolt, M. Thiele, D. Milz, M. May, R. Kuchar, and M. Hornung. Comparison of multi-fidelity rotor analysis tools for transitional and low speed flight regimes. In *Deutscher Luft- und Raumfahrtkongress 2021*, 2021. doi: 10.25967/550128.

[28] M. Tugnoli, D. Montagnani, M. Syal, G. Droandi, and A. Zanotti. Mid-fidelity approach to aerodynamic simulations of unconventional vtol aircraft configurations. *Aerospace Science and Technology*, 115, 2021. doi: 10.1016/j.ast.2021.106804.

[29] DUST project. DUST - an aerodynamics solution for complex configurations, 31.05.2022. https://www.dust-project.org/.

[30] D. Perdolt. Efficient aerodynamic modeling process for a tilt-wing evtol using a mid-fidelity computational tool: Master thesis, 2022.

[31] Z.T. Lovering, G.C. Bower, A. Stoschek, and H. Hilaire. Fault-tolerant electrical systems for aircraft, 2020.

[32] A. Savino, A. Cocco, A. Zanotti, M. Tugnoli, P. Masarati, and V. Muscarello. Coupling mid-fidelity aerodynamics and multibody dynamics for the aeroelastic analysis of rotary-wing vehicles. *Energies*, 14(21), 2021. doi: 10.3390/en14216979.

[33] D.C. Montgomery. *Design and analysis of experiments*. Eighth edition edition, 2013. ISBN 9781621982272.

[34] I. Efthimiou, S.D. Georgiou, and M. Liu. Construction of nearly orthogonal latin hypercube designs. *Metrika*, 78(1):45–57, 2015. doi: 10.1007/s00184-014-0489-5.

[35] A.S. Hernandez, T.W. Lucas, and M. Carlyle. Constructing nearly orthogonal latin hypercubes for any nonsaturated run-variable combination. *ACM Transactions on Modeling and Computer Simulation*, 22(4): 1–17, 2012. doi: 10.1145/2379810.2379813.

[36] V. Klein and E.A. Morelli. *Aircraft system identification: Theory and practice*. AIAA education series. 2006. ISBN 1563478323.

[37] P.M. Rothhaar, P.C. Murphy, B.J. Bacon, I.M. Gregory, J.A. Grauer, R.C. Busan, and M.A. Croom. Nasa langley distributed propulsion vtol tiltwing aircraft testing, modeling, simulation, control, and flight test development. In *14th AIAA Aviation Technology, Integration, and Operations Conference*, 2014. doi: 10.2514/6.2014-2999.